Lawrence Berkeley National Laboratory

Title
Pressure-induced phase transition in the AlCoCrFeNi high-entropy alloy

Permalink
https://escholarship.org/uc/item/2r36d66v

Authors
Cheng, Benyuan
Zhang, Fei
Lou, Hongbo
et al.

Publication Date
2019-03-01

DOI
10.1016/j.scriptamat.2018.10.020

Peer reviewed

Regular article

Pressure-induced phase transition in the AlCoCrFeNi high-entropy alloy

Benyuan Cheng [a,b,1], Fei Zhang [a,d,1], Hongbo Lou [a], Xiehang Chen [a], Peter K. Liaw [e,*], Jinyuan Yan [f,g], Zhidan Zeng [a], Yang Ding [a], Qiaoshi Zeng [a,c,**]

[a] Center for High Pressure Science and Technology Advanced Research, Pudong, Shanghai 201203, People's Republic of China
[b] China Academy of Engineering Physics, Mianyang 621900, Sichuan, People's Republic of China
[c] Jiangsu Key Laboratory of Advanced Metallic Materials, School of Materials Science and Engineering, Southeast University, Nanjing 211189, People's Republic of China
[d] State Key Laboratory for Advanced Metals and Materials, University of Science and Technology Beijing, Beijing 100083, People's Republic of China
[e] Department of Materials Science and Engineering, The University of Tennessee, Knoxville, TN 37996, USA
[f] Advanced Light Source, Lawrence Berkeley National Laboratory, Berkeley, CA 94720, USA
[g] Department of Earth and Planetary Sciences, University of California, Santa Cruz, Santa Cruz, CA 95064, USA

ARTICLE INFO

ABSTRACT

The recently discovered pressure-induced polymorphic transitions (PIPT) in high-entropy alloys (HEAs) have opened an avenue towards understanding the phase stability and achieving atomic structural tuning of HEAs. So far, whether there is any PIPT in the body-centered cubic (*bcc*) HEAs remains unclear. Here, we studied an ordered *bcc*-structured (B2 phase) AlCoCrFeNi HEA using *in situ* synchrotron radiation X-ray diffraction (XRD) up to 42 GPa and *ex situ* transmission electron microscopy, a PIPT to a likely-distorted phase was observed. These results highlight the effect of the lattice distortion on the stability of HEAs and extend the polymorphism into ordered *bcc*-structured HEAs.

© 2018 Acta Materialia Inc. Published by Elsevier Ltd. All rights reserved.

High-entropy alloys (HEAs) are a new class of solid solutions containing multi-principal elements (five or more) in equal or near-equal atomic ratios, which have drawn extensive attention in the metallic materials community [1–3]. Their unique compositions and atomic structures result in a combination of many superior properties for potential applications, such as high ductility and strength over a wide temperature range, and excellent resistance to wear and corrosion [4–15]. Although with complex compositions, HEAs tend to form simple solid solutions with high structural symmetry, *e.g.*, *fcc* (face-centered cubic), *bcc* (body-centered cubic), and *hcp* (hexagonal close-packing) [16]. These simple structures were found to be highly stable during heating over a large range from cryogenic temperatures up to the melting temperatures in various HEAs [4,5,13], which provide promising candidates for applications at extreme conditions. However, the high stability of HEAs is surprising considering the rich polymorphism phenomena in their typical constituent elements, such as Fe, Co, Mn, Zr, and Ti *etc.* [17] Therefore, many efforts have been made to address their extraordinary structural stability [16,18]. So far, the structural stability of HEAs is believed to be strongly associated with the deliberately maximized configurational entropy from a thermodynamic point of view, and also the kinetic factor of extremely sluggish atomic diffusion caused by the chemical-complexity induced packing disorder and considerable local lattice distortion [13,14,19–23].

Recently, by employing pressure as an alternative tuning parameter to study the phase stability of HEAs, pressure-induced phase transitions were surprisingly revealed in some HEAs by different groups. [24–28] *E. g.*, pressure-induced irreversible polymorphic transitions from the *fcc* to *hcp* phases were observed in the prototype CoCrFeMnNi HEA [24–26], and in a medium-entropy alloy system of the NiCoCrFe alloy [27]. The synthesized *hcp* CoCrFeMnNi HEA had an inverse transition from *hcp* to *fcc* structures during heating at different pressures. Therefore, it clarified that the commonly-synthesized *fcc* phase is actually stable at relatively high temperatures, while the *hcp* phase is more favorable at lower temperatures. [24] In another rare-earth system, an *hcp*-structured HoDyYGdTb HEA, more complex transitions following the sequence *hcp* → *Sm-type* → *dhcp* → *dfcc* like those typically observed in the pure rare earth elements were reported [28].

Besides the *fcc* and *hcp*, *bcc*-structured alloys (including both the chemically ordered B2 and disordered A2 phases) are the other most common HEAs that usually possess high yield strength, making them promising for structural applications. Therefore, understanding the phase stability of the *bcc* HEAs is of great importance and also has been explored under high pressure. For example, Ahmad et al. studied the compression behavior of the equimolar *bcc* TiZrHfNb and found no

* Corresponding author.
** Correspondence to: Q. Zeng, Center for High Pressure Science and Technology Advanced Research, Pudong, Shanghai 201203, People's Republic of China.
E-mail addresses: pliaw@utk.edu (P.K. Liaw), zengqs@hpstar.ac.cn (Q. Zeng).
[1] Equal contribution authors.

phase transition up to 50.8 GPa [29]; Yusenko et al. also reported that the *bcc* structure of the Al$_2$CoCrFeNi HEA was stable up to 60 GPa [30]. Guo et al. compressed the superconducting (TaNb)$_{0.67}$ (HfZrTi)$_{0.33}$ HEA up to 100 GPa, which remained in its *bcc* structure without any structural transition [31]. These results show that *bcc*-structured HEAs seem quite stable under high pressures up to at least tens of GPa, which is different from the polymorphism observed in *fcc* or *hcp* HEAs. However, the typical *bcc* structure of metallic materials has a much lower packing density (~68%), compared with that of the *fcc* or *hcp* structures (~74%); therefore, a denser structure is naturally expected under high pressure. Moreover, most of the typical *bcc*-structured metallic elements, such as alkali metals, iron, vanadium, and europium, *etc.*, show rich polymorphism at quite low pressures, mostly at ~10 GPa [17,32,33]. Thus, an intriguing and important question is raised: is polymorphism really possible in the *bcc*-structure (A2 or B2 phase) HEAs?

To address this question, we chose a prototype *bcc*-structured HEA, the equiatomic AlCoCrFeNi alloy as the model system to study the *bcc* structural evolution and possible polymorphism under high pressure using *in situ* high-pressure synchrotron X-ray diffraction (XRD). Wang et al. [34] reported that in the Al$_x$CoCrFeNi HEA system, the atomic structure is susceptible to the Al content, *e.g.*, it can possess an *fcc* structure when x < 0.5, and *bcc* (A2/B2) phases with x > 0.9, or a mixture of *fcc* and *bcc* (A2/B2) phases with 0.5 < x < 0.9. The increase of the Al content could significantly stabilize the *bcc* structure. Therefore, in this work, to lower the relative stability of the *bcc* structure and subsequently decrease the possible critical pressure required for the phase transitions, we chose the composition near the *fcc* and *bcc* boundary, the *bcc*-structured equiatomic AlCoCrFeNi HEA as a model system.

An ingot of the AlCoCrFeNi master alloy was produced by arc-melting a mixture of pure constituent elements, Al, Co, Cr, Fe, and Ni (99.99 atomic percent) under a Ti-gettered high-purity argon atmosphere. The ingot was remelted at least four times to ensure chemical homogeneity. Thin ribbon samples (~30 μm in thickness) were prepared using the single-roller melt-spinning method with a copper wheel speed of 30 m/s under an argon atmosphere to obtain samples with small grains for the high-pressure study. The crystal structure of the as-prepared melt-spun AlCoCrFeNi ribbon sample was found to be B2 (space group: *Pm-3m*) with a lattice constant $a = 2.878$ Å. Usually, a B2/A2 mixture phase was obtained for the composition AlCoCrFeNi in melt-casting and the B2:A2 volume ratio varies with the synthesis conditions [34,35]. The likely single B2 phase obtained in this work may be attributed to the ultrafast quenching rate in melt-spinning. The composition homogeneity was checked by energy-dispersive X-ray spectroscopy (EDS). A composition closed to the nominal value, and homogeneous spatial distribution was confirmed (Supplementary Fig. 1). *In situ* high-pressure angle-dispersive XRD experiments were performed on the AlCoCrFeNi ribbon sample at the beamline 12.2.2, Advanced Light Source (ALS), Lawrence Berkeley National Laboratory (LBNL), USA. The X-ray wavelength was 0.4959 Å. The detector position and orientation were calibrated using the CeO$_2$ standard. High pressure was generated using a symmetric diamond anvil cell (DAC) with a culet size of 400 μm. The gasket was the T301 stainless steel, and the pressure-transmitting medium was silicone oil. Pressures were determined using the ruby fluorescence [36]. One-dimensional (1D) XRD patterns were obtained by integrating the two-dimensional (2D) diffraction images along the azimuth angle from 0° to 360° using the Dioptas software [37].

The XRD patterns collected during both compression and decompression are shown in Fig. 1a. With increasing pressure, all the diffraction peaks shift to larger two-theta angles. Meanwhile, they also present dramatic change of both peak intensity and width. More detailed information can be found in Fig. 1b. Below 17.6 GPa, the diffraction peaks of the B2 phase show a slight intensity decrease. Above 17.6 GPa, all the peak intensities drop significantly, but not in a consistent way, *e.g.*, the (100), (200) and (111) peaks become extremely
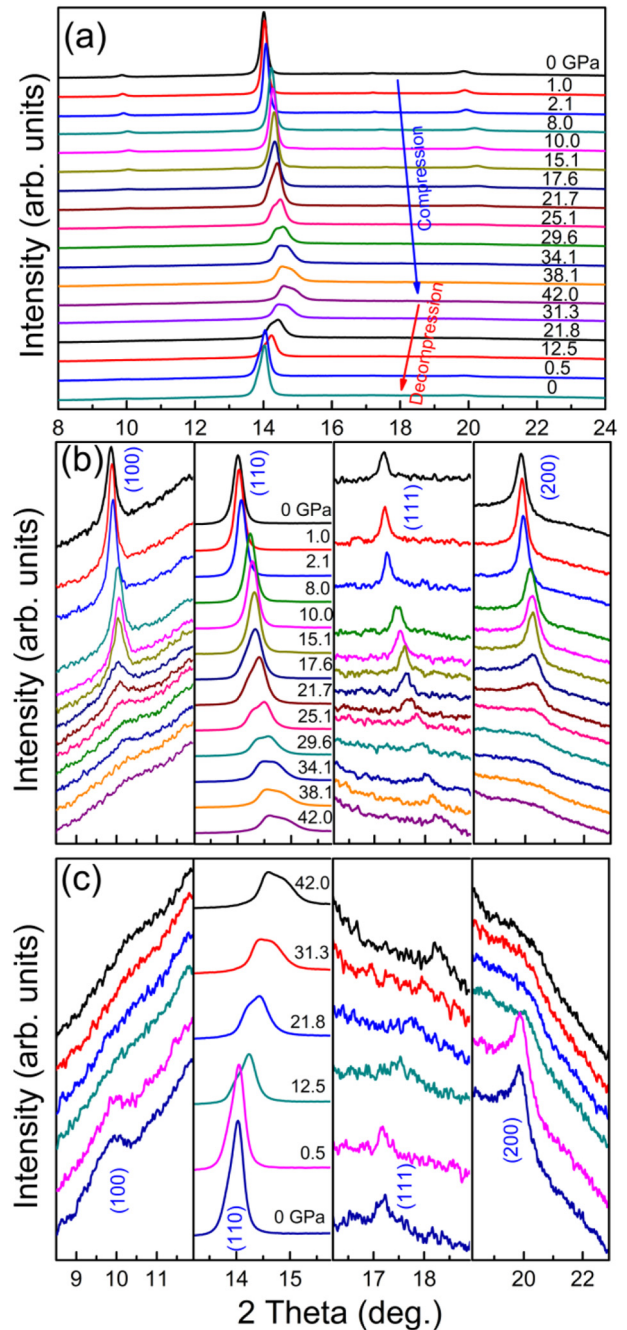

Fig. 1. *In situ* high-pressure XRD patterns of the AlCoCrFeNi HEA at room temperature during compression and decompression (a). The locally enlarged plot of the XRD patterns of each peak upon compression (b) and decompression (c). The initial B2 phase remains stable up to ~17.6 GPa upon compression, a phase transition indicated by the (110) peak splitting starting at ~17.6 GPa. The new high-pressure phase may be partially recovered to ambient pressure. The X-ray wavelength is 0.4959 Å. The number on each pattern represents the pressure.

broad and weak, the (100) and (200) peaks are almost invisible above 25 GPa. This feature is not the case for the strongest (110) peak, whose peak width increases dramatically with the pressure above 17.6 GPa, and a visible new peak emerges on its left shoulder at 17.6 GPa and gradually increases its intensity at the expense of the initial (110) peak. The relative intensity of the new peak and the initial peak starts to reverse above 34 GPa. These results suggest a high-pressure induced phase transition starts at ~17.6 GPa.

Upon decompression (see Fig. 1a and c), the (111) peak retains its peak intensity and peak width, while the other peaks gradually recover
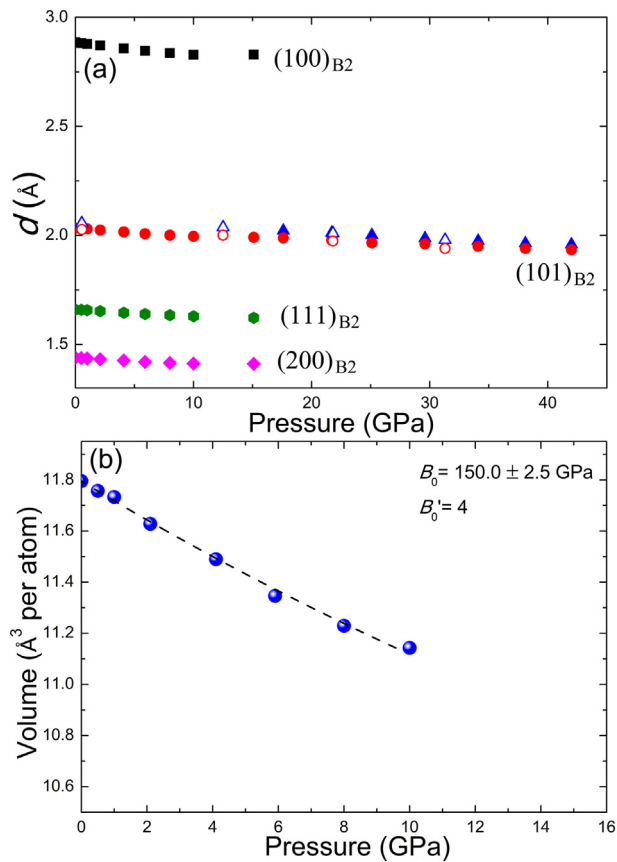
Fig. 2. Pressure dependence of the AlCoCrFeNi HEA *d*-spacings and volume. (a) The *d*-spacings associated with the major Bragg peaks of the initial B2 phase and the new phase (shown in solid blue triangle for compression and open blue triangles for decompression) change with increasing pressure. The error bars are smaller than the symbol sizes. (b) The average volume per atom for the initial B2 phase are calculated as a function of pressure. The volume data can be well fitted using the third-order Birch-Murnaghan EOS (dashed line).

their intensity, showing a seemingly reversible behavior of the compression process. However, the peak width of the (100) and (200) peaks do not go back to their initial values. Moreover, the (110) peak remains asymmetrical and split, indicating the partial reversibility of the phase transition. To confirm that this peak splitting and weakening is not associated with the specific synthesis method of melt-quenching

(extremely high quenching rate), another bulk sample obtained by the copper-mold-casting method was also studied by *in situ* high-pressure XRD with helium as the pressure medium at the beamline 16-ID-B, Advanced Photon Source (APS), Argonne National Laboratory (ANL), USA. Similar results with peak splitting and weakening were also observed with only a slight difference in the transition pressure (Supplementary Fig. 2).

The XRD peaks in Fig. 1a were fitted using a Voigt line profile and the peak positions are presented in *d*-spacings as a function of pressure in Fig. 2a. The (100), (111), and (200) peaks are only shown below 17.6 GPa because they are almost invisible above 17.6 GPa. For the (110) peak, above 17.6 GPa obvious peak splitting takes place with an extra new peak emerged with a slightly larger *d*-spacing value and coexisting with the initial (110) peak up to 42 GPa. During decompression, the split peaks almost follow the same trend as that in the compression process, suggesting a likely irreversible transition. Below 17.6 GPa, the relatively high quality XRD data of the initial B2 phase enables us to calculate the sample volume as a function of the pressure. The volume data of the initial B2 phase shown in Fig. 2b can be well fitted by the third-order Birch-Murnaghan isothermal equation of state (EOS) [38], with an isothermal bulk modulus $B_0 = 150 \pm 2.5$ GPa and its pressure derivative B_0' fixed at 4.

Due to the severe peak weakening and broadening above 17.6 GPa, the new phase after the pressure-induced phase transition of the AlCoCrFeNi HEA is challenging to be identified. The most noticeable feature of the new phase is the splitting of the (110) peak. Since no other new peaks appear and some peaks of the initial B2 phase are severely weakened, the splitting of a peak during compression could be mostly caused by a pressure-induced transition with severe lattice distortion [39]. Specifically, there are three possible scenarios: the first one is that the high-pressure phase is a mixture of the initial B2 phase and a new body-centered tetragonal (*bct*) phase, which can be viewed as a distortion of the B2 structure with a slight change of the *a/c* ratio. In this case, the peak splitting of the peak (110) should contain three peaks, namely the (110) peak of the initial B2 and the new (101) and (110) peaks of the *bct* phase. The other possibility is that the splitting of the (110) peak is caused by two (110) peaks from two B2 phases, and the two B2 phases have slightly different *d*-spacings of the (110) peaks due to distortion. The third possibility is that an *fcc* phase is stabilized by high-pressure even though its Al content is above the critical value (0.9) for the *fcc* stable zone at ambient conditions [34]. Therefore, the peak splitting may be attributed to the emergence of the *fcc* (111) peak on the left shoulder of the initial B2 (110) peak.

However, it is almost impossible to directly clarify the origin of the splitting of the (110) peak based on the existing *in situ* high-pressure
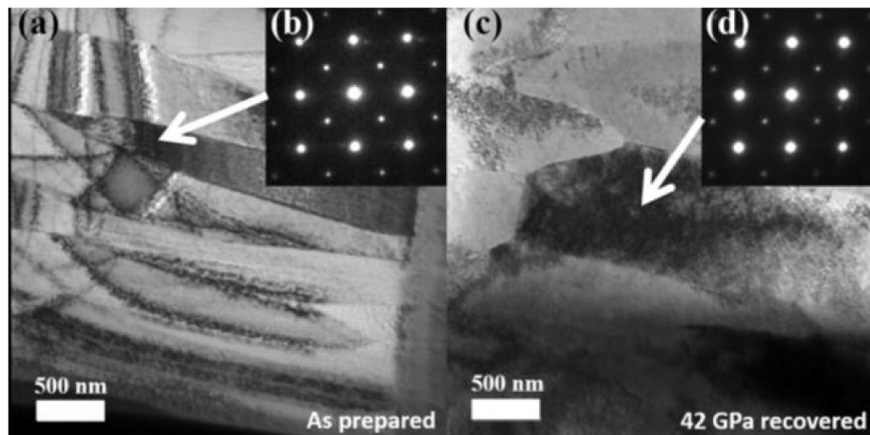

Fig. 3. Transmission electron microscopy (TEM) image and selected area electron diffraction (SAED) images of the as-prepared sample and the sample recovered from 42 GPa. The contrast of the different grains is caused by their various crystallographic orientations. The SAED data confirm that the ordered *bcc* structure (B2) phases are the major phases in the initial (b) and high pressure recovered (d) samples.
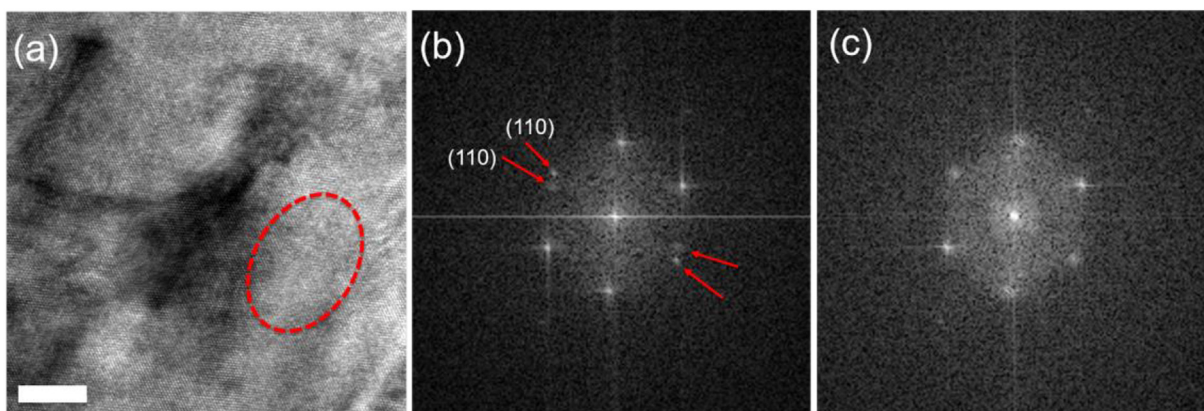
Fig. 4. An HRTEM image (a) and FFT of the local region marked by a red dashed circle (b) and of the other regions (c) in the image of the AlCoCrFeNi HEA sample recovered from 42 GPa.

XRD data with severe lattice distortion. Since the transition may be irreversible or partially reversible, we employed transmission electron microscopy (TEM) to further study the atomic structure in the sample recovered from high-pressure (JEM-2100F Field Emission Electron Microscope, 200 keV). The TEM samples were prepared by focused ion beam cutting (FEI Versa 3D). The primary phases in both the as-prepared and recovered samples are confirmed to be B2 (Fig. 3). There is no clear evidence for the existence of *bct* or *fcc* phase according to the SEAD images of several tested samples. However, in some resolution transmission electron microscopy (HRTEM) images of the recovered samples (Fig. 4), we do find that the splitting of the (110) peak can be confirmed by two pairs of slightly different (110) spots in the Fast Fourier Transform (FFT) of the HRTEM images (Fig. 4a). By carefully analyzing the HRTEM images, it is clear that the splitting of the (110) peak is associated with the seemingly disordered area, which could be caused by high-distortion of the lattice.

Since it is not clear whether the high-pressure phases could not be fully recovered to ambient conditions or not according to the *in situ* XRD data, the results obtained by TEM, HRTEM, and SAED on the recovered sample may not reflect the real or major phases under high pressure. Thus, any of the three scenarios proposed above cannot be entirely ruled out in this study. All three scenarios can cause (110) peak splitting by the lattice distortion along the same [33] planes but yield different a/c ratios, *e.g.*, $c/a = 1$ in a B2 phase, $c/a \neq 1$ in a typical *bct* phase, and $c/a = \sqrt{2}$ in an *fcc* phase [40,41]. Furthermore, the coexistence of the B2 and/or *bct* or *fcc* phases with different a/c ratios should induce a significant amount of strains and defects, which could ruin the coherence of the phase among the grains. This could explain why most of the peaks gradually diminish their intensities with pressure and nearly disappear at high pressures, except for the peak of (110). The detailed mechanism of the phase transition in the AlCoCrFeNi HEA could be much more complicated than that of typical pure elements or simple alloy systems since many aspects can be involved, including the chemical order/disorder, the considerable local atomic distortion, the magnetic states, and their evolution under high pressure [24,25]. Nevertheless, it is clear that severe lattice distortion developed during compression plays an essential role in the phase transitions and structural destabilization observed in the B2 AlCoCrFeNi HEA. This result is consistent with the previous theoretical studies that the lattice distortion effect is more significant in the *bcc*- than the *fcc*-structured HEAs and the local lattice distortion is sensitive to pressure [20,21]. In an effective elastic medium model of chemically disordered equimolar complex alloys proposed by Ye et al., the atomic scale lattice distortion are revealed to build up a non-symmetric residual strain field with atomic scale fluctuations [23], and this kind of non-symmetric residual strain field is usually regarded as a direct cause to induce a potential phase transition.

In summary, we studied the atomic structural evolution of the ordered *bcc*-structured (B2) AlCoCrFeNi HEA during compression up to 42 GPa and a followed decompression process to ambient pressure using *in situ* synchrotron radiation XRD in a DAC. We observed peak splitting of the (110) peak, and peak broadening and weakening of the other peaks above ~17.6 GPa. Upon decompression, the high-pressure phase may be partially recovered to the ambient conditions. Combining *ex situ* HRTEM with *in situ* XRD data, we discussed the possible atomic structure of the high-pressure phases and the possible mechanism, and believe the phase transition is closely associated with severe lattice distortion in the {110} planes of the initial B2 phase. A pressure-induced polymorphic phase transition in a *bcc*-structured (ordered B2 phase) HEA has been observed. However, the atomic structure of the high pressure phase is not conclusive in this work and requires the help of theoretical simulations in the future. Considering the pressure-induced phase transitions that have been previously reported in *fcc* and *hcp* HEAs, we expect that polymorphism may be a common phenomenon in various HEAs. Pressure could be a powerful tool for understanding the structural stability and lattice distortion of HEAs, and also synthesizing novel HEAs, which are otherwise not readily obtainable by other means.

Appendix A. Supplementary data

See supplementary material for the composition analysis of the initial sample using EDS and the *in situ* high-pressure XRD patterns of

another bulk sample synthesized by the copper-mold-casting. Supplementary data to this article can be found online at doi:https://doi.org/10.1016/j.scriptamat.2018.10.020.

References

[1] B. Cantor, I.T.H. Chang, P. Knight, A.J.B. Vincent, Mater. Sci. Eng. A 375–377 (2004) 213–218.
[2] Y. Zhang, X. Yang, P.K. Liaw, JOM 64 (7) (2012) 830–838.
[3] J.W. Yeh, S.K. Chen, S.J. Lin, J.Y. Gan, T.S. Chin, T.T. Shun, C.H. Tsau, S.Y. Chang, Adv. Eng. Mater. 6 (2004) 299–303.
[4] F. Otto, A. Dlouhy, C. Somsen, H. Bei, G. Eggeler, E.P. George, Acta Mater. 61 (15) (2013) 5743–5755.
[5] B. Gludovatz, A. Hohenwarter, D. Catoor, E.H. Chang, E.P. George, R.O. Ritchie, Science 345 (6201) (2014) 1153–1158.
[6] S. Praveen, H.S. Kim, Adv. Eng. Mater. (2017) 1700645.
[7] N. Stepanov, M. Tikhonovsky, N. Yurchenko, D. Zyabkin, M. Klimova, S. Zherebtsov, A. Efimov, G. Salishchev, Intermetallics 59 (Supplement C) (2015) 8–17.
[8] Y. Zou, H. Ma, R. Spolenak, Nat. Commun. 6 (2015) 7748.
[9] Z.J. Zhang, M.M. Mao, J.W. Wang, B. Gludovatz, Z. Zhang, S.X. Mao, E.P. George, Q. Yu, R.O. Ritchie, Nat. Commun. 6 (2015) 10143.
[10] O.N. Senkov, G.B. Wilks, J.M. Scott, D.B. Miracle, Intermetallics 19 (5) (2011) 698–706.
[11] M.H. Chuang, M.H. Tsai, W.R. Wang, S.J. Lin, J.W. Yeh, Acta Mater. 59 (16) (2011) 6308–6317.
[12] Y.Z. Shi, B. Yang, X. Xie, J. Brechtl, K.A. Dahmen, P.K. Liaw, Corros. Sci. 119 (2017) 33–45.
[13] W.H. Liu, Y. Wu, J.Y. He, T.G. Nieh, Z.P. Lu, Scr. Mater. 68 (7) (2013) 526–529.
[14] K.Y. Tsai, M.H. Tsai, J.W. Yeh, Acta Mater. 61 (13) (2013) 4887–4897.
[15] D.B. Miracle, O.N. Senkov, Acta Mater. 122 (2017) 448–511.
[16] Y. Zhang, T.T. Zuo, Z. Tang, M.C. Gao, K.A. Dahmen, P.K. Liaw, Z.P. Lu, Prog. Mater. Sci. 61 (2014) 1–93.
[17] E.Y. Tonkov, E.G. Ponyatovsky, Phase Transformations of Elements Under High Pressure, CRC Press, 2004.
[18] S. Guo, C.T. Liu, Prog. Nat. Sci. Mater. Int. 21 (6) (2011) 433–446.
[19] Z.J. Wang, Y.H. Huang, Y. Yang, J.C. Wang, C.T. Liu, Scr. Mater. 94 (2015) 28–31.
[20] H. Song, F. Tian, Q.-M. Hu, L. Vitos, Y. Wang, J. Shen, N. Chen, Phys. Rev. Mater. 1 (2) (2017) 023404.
[21] H. Oh, D. Ma, G. Leyson, B. Grabowski, E. Park, F. Körmann, D. Raabe, Entropy 18 (9) (2016) 321.
[22] Z. Wang, W. Qiu, Y. Yang, C.T. Liu, Intermetallics 64 (2015) 63–69.
[23] Y.F. Ye, Y.H. Zhang, Q.F. He, Y. Zhuang, S. Wang, S.Q. Shi, A. Hu, J. Fan, Y. Yang, Acta Mater. 150 (2018) 182–194.
[24] F. Zhang, Y. Wu, H.B. Lou, Z.D. Zeng, V.B. Prakapenka, E. Greenberg, Y. Ren, J.Y. Yan, J.S. Okasinski, X.J. Liu, Y. Liu, Q.S. Zeng, Z.P. Lu, Nat. Commun. 8 (2017) 15687.
[25] C.L. Tracy, S. Park, D.R. Rittman, S.J. Zinkle, H.B. Bei, M. Lang, R.C. Ewing, W.L. Mao, Nat. Commun. 8 (2017) 15634.
[26] E.W. Huang, C.M. Lin, J. Jain, S.R. Shieh, C.P. Wang, Y.C. Chuang, Y.-F. Liao, D.Z. Zhang, T. Huang, T.N. Lam, W. Woo, S.Y. Lee, Mater. Today Commun. 14 (2018) 10–14.
[27] F.X. Zhang, S.J. Zhao, K. Jin, H.B. Bei, D. Popov, C.Y. Park, J.C. Neuefeind, W.J. Weber, Y.W. Zhang, Appl. Phys. Lett. 110 (1) (2017) 011902.
[28] P.F. Yu, L.J. Zhang, J.L. Ning, M.Z. Ma, X.Y. Zhang, Y.C. Li, P.K. Liaw, G. Li, R.P. Liu, Mater. Lett. 196 (2017) 137–140.
[29] A.S. Ahmad, Y. Su, S.Y. Liu, K. Ståhl, Y.D. Wu, X.D. Hui, U. Ruett, O. Gutowski, K. Glazyrin, H.P. Liermann, H. Franz, H. Wang, X.D. Wang, Q.P. Cao, D.X. Zhang, J.Z. Jiang, J. Appl. Phys. 121 (23) (2017) 235901.
[30] K.V. Yusenko, S. Riva, W.A. Crichton, K. Spektor, E. Bykova, A. Pakhomova, A. Tudball, I. Kupenko, A. Rohrbach, S. Klemme, F. Mazzali, S. Margadonna, N.P. Lavery, S.G.R. Brown, J. Alloys Compd. 738 (2018) 491–500.
[31] J. Guo, H. Wang, F. von Rohr, Z. Wang, S. Cai, Y. Zhou, K. Yang, A. Li, S. Jiang, Q. Wu, R.J. Cava, L. Sun, Proc. Natl. Acad. Sci. U. S. A. 114 (50) (2017) 13144–13147.
[32] Y. Ding, R. Ahuja, J. Shu, P. Chow, W. Luo, H.-k. Mao, Phys. Rev. Lett. 98 (8) (2007) 085502.
[33] W. Bi, Y. Meng, R.S. Kumar, A.L. Cornelius, W.W. Tipton, R.G. Hennig, Y. Zhang, C. Chen, J.S. Schilling, Phys. Rev. B 83 (10) (2011) 104106.
[34] W.R. Wang, W.L. Wang, S.C. Wang, Y.C. Tsai, C.H. Lai, J.W. Yeh, Intermetallics 26 (2012) 44–51.
[35] Y.F. Kao, T.J. Chen, S.K. Chen, J.W. Yeh, J. Alloys Compd. 488 (1) (2009) 57–64.
[36] H.K. Mao, J. Xu, P.M. Bell, J. Geophys. Res. Sol. Earth 91 (B5) (1986) 4673–4676.
[37] C. Prescher, V.B. Prakapenka, High Pressure Res. 35 (3) (2015) 223–230.
[38] B. Francis, J. Geophys. Res. 57 (2) (1952) 60.
[39] Q. Guo, Y. Zhao, W.L. Mao, Z. Wang, Y. Xiong, Y. Xia, Nano Lett. 8 (3) (2008) 972–975.
[40] Y. Xie, Y.M. Ma, T. Cui, Y. Li, J. Qiu, G.T. Zou, New J. Phys. 10 (6) (2008) 063022.
[41] V.F.D.O. Degtyareva, F. Porsch, W.B. Holzapfel, J. Phys. Condens. Matter 13 (2001) 7295.